Title
The effect of the Drosophila melanogaster Fhod tail on actin assembly

Author
Bremer, Kathryn Victoria

Publication Date
2019

Peer reviewed|Thesis/dissertation

UNIVERSITY OF CALIFORNIA

Los Angeles

The effect of the *Drosophila melanogaster* Fhod tail on actin assembly

A thesis submitted in partial satisfaction

of the requirements for the degree Master of Science

in Biochemistry, Molecular and Structural Biology

by

Kathryn Victoria Bremer

2019

ABSTRACT OF THE THESIS

The effect of

the *Drosophila melanogaster* Fhod tail

on actin assembly

by

Kathryn Victoria Bremer

Master of Science in Biochemistry, Molecular and Structural Biology

University of California, Los Angeles, 2019

Professor Margot Elizabeth Quinlan, Chair

Formin-family proteins are a diverse group of proteins that accelerate actin nucleation and elongation. Understanding the dynamics and biochemical nature of proteins that assist in actin assembly can provide insight into normal development, as well as dystrophies, cardiomyopathies, and cancer. Formins are defined by their homodimeric Formin Homology (FH) 2 domain and proline-rich FH1 domain. The FH2 domain binds to the fast-growing barbed-end of actin filaments and the FH1 domain delivers profilin-bound actin to the FH2 domain, accelerating elongation. The *Drosophila melanogaster* Formin Homology Domain (Fhod) protein is important in muscle development, tracheal development and macrophage motility. We previously reported that Fhod isoform A nucleates, protects barbed-ends, and bundles actin

filaments. Here, we show the analysis of constructs designed to characterize the variable C-terminal tail of Fhod. Formin tails alter both nucleation and elongation activity, and must be considered in conjunction with the FH1 and FH2 domains.

The thesis of Kathryn Victoria Bremer is approved.

Emil Reisler

Jorge Torres

Margot Elizabeth Quinlan, Committee Chair

University of California, Los Angeles

2019

Table of Contents

Section *Page Number*

List of Figures and Tables

Figure/Table *Page Number*

Acknowledgments

First and foremost, I would like to thank my mentors Dr. Margot E. Quinlan and Aanand A. Patel. I came to UCLA as a transfer student. I was introduced to the Quinlan Lab by Dr. Rachel Kennison, who at the time was the head of a summer internship program between UCLA and Santa Monica College. During my summer internship, I quickly realized that I wanted to remain in the lab for the rest of my time at UCLA. Both Margot and Aanand were dedicated and patient mentors. They worked with me to understand different biochemical concepts and techniques. Even more, along with the lab, they welcomed me and made me feel at home. During that first summer, I asked Aanand on several occasions, "do you think that she will keep me?" I was ecstatic to find that answer to be "yes". It is because of Margot and Aanand that I entered both the Biomedical Research Minor and the Chemistry and Biochemistry Departmental Scholars Program. Instead of graduating with a Bachelor of Science in Chemistry, I am graduating with a Bachelor of Science in Biochemistry, a minor in Biomedical Research, and a Master of Science in Biochemistry, Molecular and Structural Biology. Without them I would certainly have missed the opportunity to reach my full potential at UCLA. I am forever grateful to Margot and Aanand for paving the path they helped me travel on. I wish I had the space to thank everyone in the Quinlan Lab individually, however, there is a lot of awesome science to get to. I would like to thank Nicole Lynn for her hard work in protein expression and purification. Everyone in the Quinlan Lab has been important to my growth as a scientist and person. The people that Margot attracts and selects speak to her outstanding character.

I would also like to thank the members on my Thesis Committee, Dr. Jorge Torres and Dr. Emil Reisler, for taking the time to support my education. I had more frequent interactions

with Dr. Reisler and will never forget his wisdom and humor. He never failed at putting a smile on my face with a science joke or a reminder not to take life too seriously.

My parents and sister have also been a huge inspiration to my academic journey. As someone who returned to college after a LONG hiatus from school, my family continuously pushed me to do my best. My mother and father met during college. My sister followed in our mother's footsteps earning her degree in English, whereas I followed my father's footsteps. He majored in Biology and minored in Chemistry. They have been so supportive of my college education and their belief in me has kept me going. While in the Quinlan Lab, I have started a family of my own. Rasha Abed has been my strength and my heart. She has been so proud of my accomplishments and is the foundation I have been supported by for the past year and half. She and her son have been my home, my family, and have given me a greater purpose. Life does not happen in a vacuum. This work reflects all the people that have supported me. It takes a village.

Figure 1.1 was originally published in the Annual Review of Biochemistry: Goode BL and Eck MJ. Mechanism and function on formins in the control of actin assembly. *Annu Rev Biochem.* 2007; 76: 593-627. © Annual Reviews. Figure 1.2 was originally published in the European Journal of Cell Biology: Randall TS and Ehler E. A formin-g role during development and disease. *Eur J Cell Biol*. 2014; 93: 205-211. © Elsevier Inc. Figure 1.3 was originally published in Trends in Biochemical Sciences: Higgs HN. Formin proteins: a domain-based approach. *Trends in Biochem Sci*. 2005; 30: 342-353. © Elsevier Inc. Figure 3.2B was originally published in the Journal of Biological Chemistry: Patel AA, Oztug Durer ZA, van Loon AP, Bremer KV, and Quinlan ME. Drosophila and human FHOD family formins nucleate actin filaments. *J Biol Chem*. 2018; 293: 532-540. © The American Society for Biochemistry and Molecular Biology.

Chapter One: Introduction

1.1 Objective

We seek to address the effect of the Fhod tail domain on actin assembly by probing three different splice isoforms that differ only by the tail domain (Fhod-A, -B, -E). By expressing and purifying C-terminal constructs of these isoforms and mutant constructs that are intermediate in length between Fhod-A and Fhod-B we can determine the impact of the tail on nucleation, elongation, and processivity. This work will provide a detailed analysis of the tail domains and their varying effects on actin assembly. We proposed a model in which the tail acts via direct interaction with the sides of growing actin filaments.

1.2 Literature review

1.2a Actin cytoskeleton

Actin monomers non-covalently polymerize to form helical filaments that subsequently form higher-order structures in the cell such as the cleavage furrow and microvilli (Holmes et al., 1990; Oda et al., 2009; Chhabra & Higgs, 2007; Schönichen & Geyer, 2010). The formation of higher-order structures via polymerization dynamics has vital effects on development, cell structure, cell motility, and muscle contraction. The assembly of filamentous actin (F-actin) from monomeric globular actin (G-actin), including nucleation and elongation, is necessary for actin to function within these roles (Pollard & Cooper, 2009). For elongation of filaments to proceed, a stable nucleus must form. However, spontaneous actin assembly is kinetically unfavorable due to the instability of actin dimers and trimers (Figure 1.1; Goode & Eck, 2007). Actin filament polarization is established by monomers adding in the same direction. Although monomers can

add to filaments at both the pointed-end and barbed-end, both polymerization and de-polymerization occur more than ten times faster at the barbed-end. In the presence of profilin, addition of monomers is restricted to the barbed-end (Chhabra & Higgs, 2007).

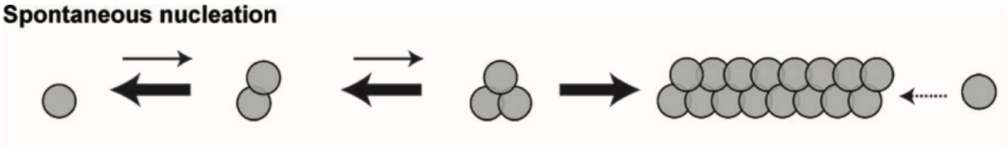

Figure 1.1: Spontaneous nucleation and subsequent elongation of actin filaments. Actin dimers and trimers are unstable and rapidly dissociate. A stable nucleus must form for elongation to proceed. *Note:* Figure is reprinted from (Goode & Eck, 2007).

Different classes of accessory proteins assist in actin nucleation and elongation, enabling a more kinetically favorable assembly to meet cellular demands (Schönichen & Geyer, 2010). Depending on the specific accessory proteins interacting with actin monomers and filaments, different mechanisms are employed to generate function-specific actin structures. Over 100 accessory proteins have been identified that regulate assembly, polymerization, the turnover of actin filaments, bundling, and filament cross-linking (Pollard & Cooper, 2009).

1.2b Formin classification and function

Formins are a large and highly conserved multidomain protein family that nucleates actin and modifies elongation by remaining processively associated with the fast-growing barbed-end of the actin filament (Chhabra & Higgs, 2007). They are defined by their proline-rich formin homology (FH) 1 domain and homodimeric FH2 domain (Randall & Ehler, 2014). The FH2 dimerization creates a torus-like shape to facilitate nucleation and processive binding to the barbed-end of elongating filaments (Goode & Eck, 2007). The proline-rich FH1 domain recruits profilin-bound actin monomers and delivers them to the FH2 domain, enhancing the actin assembly rate (Figure 1.2; Courtemanche & Pollard, 2012; Paul & Pollard, 2008).

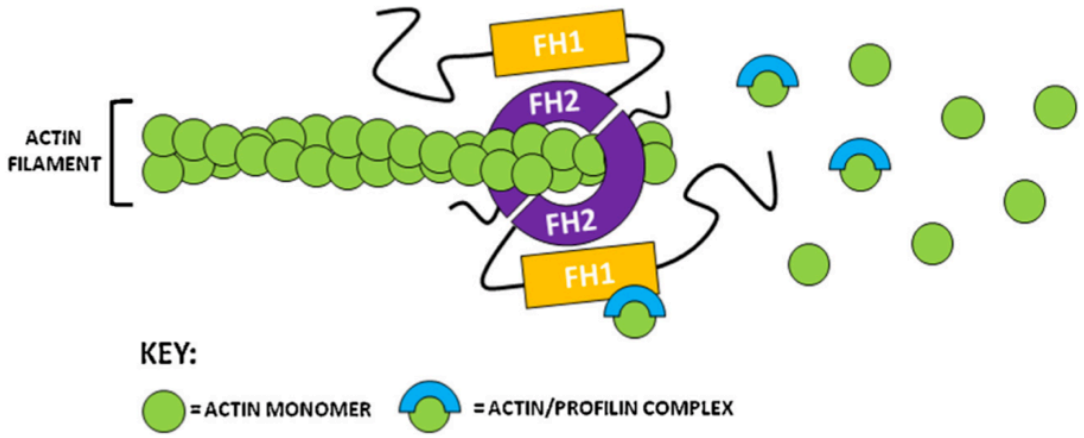

Figure 1.2: Formin-mediated actin assembly. Formins function to overcome kinetic instability of actin nucleation and accelerate elongation of growing filaments. The torus-shaped FH2 domain dimer associates with actin and stabilizes nucleation. The FH1 domain facilitates elongation by delivering profilin-bound actin to the FH2 domain which remains processively associated with the growing filament. The tail domain is located C-terminal to the FH2 domain and has been determined to alter both nucleation and processivity. *Note:* Figure is reprinted from (Randall & Ehler, 2014).

Mammals contain seven families of formins (Figure 1.3; Higgs, 2005), identified based on FH2-domain similarities: Diaphanous-related proteins (Dia), the Disheveled-associated activators of morphogenesis (DAAM), the formin-like proteins (FMNL also known as FRL), the inverted formins (INF), the formin homology domain proteins (FHOD), formin (FMN), and the delphilin proteins (Schönichen & Geyer, 2010). The importance of formins has been identified through the growing number of known formin-dependent cellular actin structures that include cleavage furrows, sarcomeres, and filopodia (Kovar et al., 2006; Chang et al., 1997; Severson et al., 2002). Though most formins assist in actin nucleation and accelerate elongation, additional formin effects on actin filaments include severing, bundling, capping, or cross-linking to microtubules (Goode & Eck, 2007). Formins differ in their ability to alter actin assembly, ability to modify actin filaments, and modes of regulation. In addition, formin activities can be restricted to either sarcomeric or cytoplasmic actin isoforms (Patel et al., 2018; Silkworth et al.,

2018). These differences account for the range of cellular actin structures that formin family proteins assist in building.

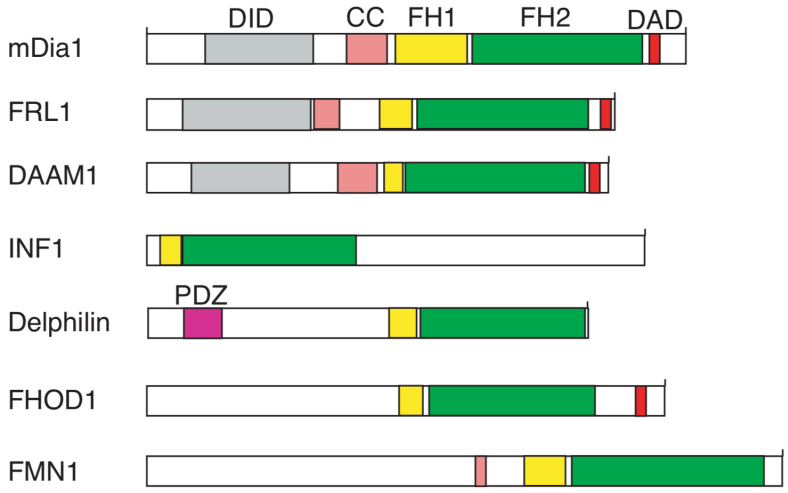

Figure 1.3: Domain structures of the seven mammalian formin families. Indicated are domains present within each of the formin families. Formins are defined by their FH1 and FH2 domains (yellow and green, respectively). Domains that vary between formin families include the diaphanous inhibitory domain (DID, grey), coiled-coil domain (CC, peach), diaphanous auto-regulatory domain (DAD, red), and Psd-95/Dlg/Zo-1 domain (PDZ, pink). *Note:* Figure is reprinted from (Higgs, 2005).

Processivity differences are also important in the consideration of the distinct cellular roles for each formin and do not correlate with the effect of acceleration on elongation. Some formins remain strongly associated with the barbed-end of growing filaments. Some formins do not remain associated with the barbed-end after nucleation, instead they may move to the sides of filaments (Goode & Eck, 2007). Barbed-end affinity presumably contributes to differences in processivity, which leads to the diverse number of cellular actin structures.

1.2c FHOD protein family

The Formin Homology Domain protein (FHOD) family includes two mammalian isoforms, Fhod1 and Fhod3. Fhod1 regulates stress fiber formation. Stress fibers are contractile units found in non-muscle cells composed of actin bundles, myosin II, and other crosslinking

proteins. Fhod1 was previously reported to inhibit actin assembly, as opposed to nucleating actin (Schönichen et al., 2013). However, we determined that Fhod1 preferentially associates with and nucleates cytoplasmic (non-muscle) actin, but not sarcomeric (muscle) actin, showing that previous findings of inhibition were due to the isoform specificity of Fhod1 (Patel et al., 2018). Interestingly, this finding is consistent with Fhod1's reported cellular roles, building non-sarcomeric structures in both muscle and non-muscle cells (Al Haj et al., 2015; Dwyer et al., 2014). The expression of Fhod3 is chiefly restricted to striated muscle and localizes to the sarcomeres of cardiomyocytes where it is required for their assembly and maintenance (Krainer et al., 2013; Iskratsch et al. 2010).

The *Drosophila melanogaster* FHOD family protein homolog, referred to here as Fhod (also known as Fhos or Knittrig) is alternatively spliced into eight isoforms that differ in their N-termini and C-terminal tails but maintain constant FH1 and FH2 domains (Bechtold et al., 2014). Fhod contributes to myofibril assembly (Shwartz et al., 2016), tracheal development, and macrophage motility (Lammel et al., 2014). Consistent with its cellular roles, Fhod nucleates both muscle and non-muscle actin. We previously reported that Fhod isoform A (Fhod-A) nucleates, protects barbed-ends, and bundles actin filaments. While it is weakly processive, Fhod-A does not appear to accelerate barbed-end actin elongation *in vitro*. Some of our results suggested that Fhod-A slows elongation; however, we attributed the decrease in elongation rate to artifacts observed with high Fhod-A concentrations in the fluorescence assay, likely due to filament bundling (Patel et al. 2018).

The extensive characterization of FHOD family formins is of interest due to their critical cellular functions. We seek to further understand the mechanisms by which both *Drosophila melanogaster* Fhod and its human homologs contribute to actin assembly.

1.2d Drosophila melanogaster Fhod tail domain

The tail domain is loosely defined and refers to the region between the FH2 domain and C-terminus in formins. The tail varies significantly in length across formins and between isoforms of the same formin (Vizcarra et al., 2014). The tail of some formins contains the diaphanous auto-regulatory domain (DAD) which interacts with the N-terminal diaphanous inhibitory domain (DID) to regulate formin activity via auto-inhibition (Higgs, 2005). The DAD is not required for auto-inhibition and there is evidence that the DID may interact weakly with the FH2 domain as well (Li & Higgs, 2005).

Earlier work in our lab characterizing another formin, Cappuccino (Capu), demonstrated that the tail region directly interacts with growing filaments and influences their processivity and nucleation (Vizcarra et al., 2014). This work showed that gradual truncation of the Capu tail resulted in a gradual decrease in processivity. Additionally, tail-less Capu has significantly diminished ability to nucleate actin. Interestingly, the tail region does not have large effects on elongation rate. When compared to our findings with Fhod-A, we were interested in determining how the Fhod tail contributes to actin activity. Wild-type Capu has a characteristic run length of 300 ± 40 μm (Yoo et al., 2015), whereas Fhod-A was found to have a characteristic run length of 2 μm (Patel et al., 2018). Of the eight *Drosophila melanogaster* Fhod isoforms, four differ only in their tail domains (Bechtold et al., 2014). The Fhod isoform B (Fhod-B) tail is 30 residues, which is the same length as the Capu tail. This interested us as Fhod-A has a tail that is 129 residues in length. We hypothesized that the size of the Fhod-A tail may be hindering association with the barbed-end of filaments.

1.3 Experimental approach

To better understand how the Fhod tail interacts with growing filaments to alter actin assembly we purified constructs of Fhod containing the FH1, FH2, and tail domains. We did so with Fhod-A, Fhod-B, and Fhod-E. We also purified Fhod-A tail truncations that have tail lengths intermediate between Fhod-A and Fhod-B (Figure 1.4).

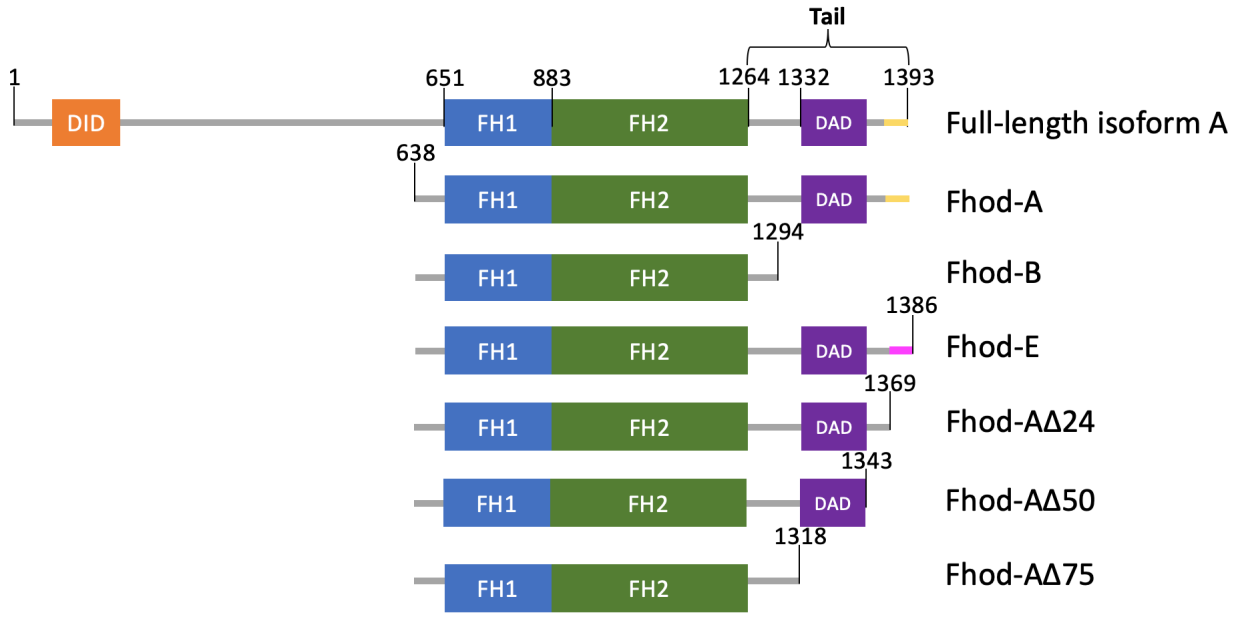

Figure 1.4: Domain structures of *Drosophila* Fhod isoform A and C-terminal constructs used for *in vitro* analysis. Full length Fhod isoform A contains the DID (orange), FH1 and FH2 domains (blue and green, respectively), and a tail domain containing a DAD motif (purple). N-terminal to the FH1 domain Fhod isoforms A, B, and E are identically spliced. Fhod isoform B terminates prior to the DAD motif at residue 1294. Fhod isoforms A and E are alternatively spliced and tail variance begins at residue 1369. The differences between the Fhod-A and Fhod-E tails are indicated in yellow and pink, respectively. Fhod-A tail truncation construct schematics are shown. Fhod-AΔ24 is truncated at the residue in which sequence variation between Fhod-A and Fhod-E begins. The tail is gradually truncated by ~25 amino acids for each additional construct.

We utilized both pyrene-labeled actin polymerization assays and TIRF microscopy experiments to quantify differences in actin assembly in the presence of these constructs. Pyrene assays were performed to determine bulk differences in actin assembly, whereas TIRF microscopy was utilized to visualize individual filaments. We exploited the preferential binding

of Chic (*Drosophila* profilin) to unlabeled actin in single filament TIRF microscopy assays. Labeling actin at Cys-374 reduces binding affinity for Chic (Vizcarra et al., 2014). The FH1 domain of formins delivers profilin-bound actin to the FH2 domain for incorporation into growing filaments. As such, filaments associated with a formin appear dim as they preferentially add unlabeled actin allowing us to quantify differences in both elongation and processivity.

Chapter Two: Materials and Methods

2.1 Protein expression and purification

All constructs were built from Fhod isoform A cDNA (SD08909, obtained from the *Drosophila* Genomics Resource Center). The cDNA was used as a template to clone C-terminal constructs into either a modified version of the pET-15b plasmid with an N-terminal His_6 tag (Fhod-A, Fhod-AΔ24, Fhod-AΔ50, Fhod-AΔ75, and Fhod-E) or a pGEX-6P-2 plasmid (Fhod-B). Fhod isoform E was cloned using Gibson Assembly. All truncated tail constructs were produced via FastCloning (Li et al., 2011) using DH5α competent cells. Fhod constructs were transformed in Rosetta I (DE3) cells (Novagen), which were grown in 1 liter of Terrific Broth (TB) supplemented with 100 mg/L and 32 mg/L of ampicillin and chloramphenicol, respectively. Expression was induced by adding 0.25 mM isopropyl β-D-thiogalactoside at an OD of 0.6-0.8 and cultures were shaken at 18ºC overnight. The cells were harvested via centrifugation, washed in PBS, flash froze in liquid nitrogen, and stored at -80ºC.

Cell pellets expressing Fhod were thawed in extraction buffer (10 mM MOPS, pH 7.0, 150 mM NaCl, 1 mM DTT, 1 mM PMSF, and 2 ug/mL DNaseI). All subsequent purification steps were conducted on ice or at 4ºC. Cells were lysed by microfluidizing and cellular debris was removed by centrifugation at 20,000xg for 20 min, and thereafter each protein was purified as described below.

Fhod-A, Fhod-AΔ24, Fhod-AΔ50, Fhod-AΔ75, and Fhod-E: Purification was carried out using the same technique as described (Patel et al., 2018). In brief, these constructs were purified using a HitrapSP-FF cation exchange column (GE Life Sciences) followed by a MonoQ anion exchange column (GE Life Sciences). Peak fractions were dialyzed into storage buffer (10 mM

Tris, pH 8.0, 150 mM NaCl, 1 mM DTT). The purified constructs were aliquoted, flash frozen using liquid nitrogen, and stored at -80ºC (Figure 2.1).

Fhod-B: Purification was carried out using glutathione sepharose resin. After one-hour rocking with glutathione sepharose resin, the lysate was poured onto a column and washed using PBS buffer. 15-mL of glutathione elution buffer (50 mM Tris, 50 mM NaCl, and 20 mM reduced glutathione at pH 8.0) was used to elute Fhod-B. The eluated protein was dialyzed in PBS with 1 mM DTT and cleaved with Precission Protease overnight. The cleaved protein was filtered through glutathione sepharose and dialyzed into 10 mM Tris, pH 8.0 50 mM NaCl, 1 mM DTT. It was next run on a MonoQ anion exchange column (GE Life Science). Peak fractions were dialyzed into Fhod storage buffer (10 mM Tris, pH 8.0, 150 mM NaCl, 1 mM DTT). The purified construct was aliquoted, flash frozen using liquid nitrogen, and stored at -80ºC (Figure 2.1).

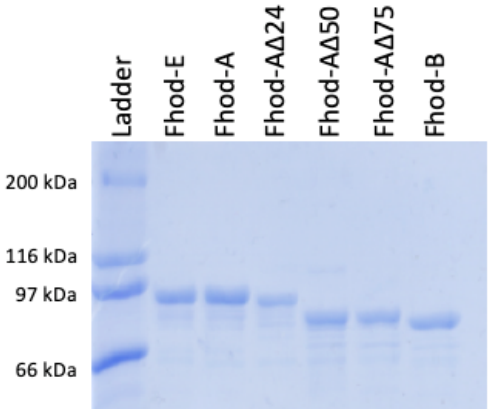

Figure 2.1: Coomassie-stained 10% SDS-PAGE of purified constructs used for *in vitro* analysis. Final purified proteins were diluted from stock concentration to 2 μM.

2.2 Pyrene-labeled actin polymerization and elongation assays

Bulk pyrene-actin polymerization assays were performed on an Infinite 200 Pro plate reader (Tecan) essentially as described (Bor et al., 2012). In brief, 2 μM 5% pyrene-labeled G-

actin was incubated for 2 min in ME buffer (200 µM ethylene glycol tetraacetic acid [EGTA] and 50 µM $MgCl_2$) to convert Ca^{2+}-actin to Mg^{2+}-actin. Polymerization was initiated by adding KMEH buffer (final concentration: 10 mM Na-HEPES, 1 mM EGTA, 50 mM KCl, and 1 mM $MgCl_2$) to the Mg^{2+}-actin. Fhod constructs were added to the KMEH buffer before addition to Mg^{2+}-actin. Calculations for $t_{1/2}$ values were performed as described (Doolittle et al., 2013).

Pyrene-labeled assays in the presence of preformed filaments (seeds) and profilin were performed to measure bulk differences in elongation rate. Final concentrations for seeded elongation assays were 2 µM G-actin (10% pyrene-labeled), 0.25 µM F-actin (seeds), and 5 µM *S. pombe* profilin. Seeds were sheared by passing three times through a 24-guage needle after an hour of benchtop polymerization. Elongation rates were determined by linear regression over the first 100 s and normalized against the rate of actin alone for each experiment. The affinity of Fhod-B for the barbed-ends was determined by fitting the data to the simplified binding equation, $r = [\text{Fhod-B}]/([\text{Fhod-B}] + K_d)\times a+b$, where r is the normalized elongation rate.

2.3 Total internal reflection fluorescence (TIRF) microscopy

TIRF microscopy was utilized to visualize individual actin filaments in real time to measure elongation rate and processivity of the Fhod constructs. Biotinylated coverslips were prepared as described (Patel et al., 2018). Flow chambers of ~15 µm were assembled on slides with strips of double-sided tape. Flow chambers were prepared with the following steps: 1) incubated for 2 min with block containing 25 µl of 1% Pluronic F-127 (Sigma), 50 µg/ml casein in PBS; 2) washed with 25 µl of 1×KMEH; 3) Incubated for 1 min with 25 µl of 40 nM streptavidin in 1×KMEH; 4) washed with 25 µl of 1×TIRF buffer (1×KMEH, 0.5% methylcellulose (400 cP, Sigma), 50 mM DTT, 0.2 mM ATP, 20 mM glucose). Oregon green-labeled G-actin in the presence of *Drosophila* profilin (Chic) was incubated for 2 min in ME

buffer (200 μM ethylene glycol tetraacetic acid (EGTA) and 50 μM $MgCl_2$) to convert Ca^{2+}-actin to Mg^{2+}-actin. The final concentrations in the flow chambers were as follows: 1 μM Mg^{2+}-G-actin (20% Oregon green labeled) in 1×KMEH, 5 μM Chic, 0.5 nM indicated Fhod construct, 0.5 nM F-actin seeds (1% biotinylated, stabilized with Alexa Fluor 647-phalloidn), 250 μg/ml glucose oxidase, 50 μg/ml catalase, and 50 μg/ml casein in 1×TIRF buffer. Fhod was incubated with seeds 45 s prior to addition of Mg^{2+}-G-actin. Growing filaments were visualized on a DMI6000 TIRF microscope (Leica, Germany) with an HCX PL APO objective (100× magnification, N.A. = 1.47), and an Andor DU-897 camera, using the Leica application suite advanced fluorescence software. Experiments were performed at room temperature. Images were captured at 10 s intervals for 10 min.

Filament lengths were quantified with the JFilament plug-in in FIJI (Smith et al., 2010). Elongation rates were calculated via the following conversion:
elongation rate (subunits s^{-1}) = length (pixels s^{-1})×0.16 (μm $pixel^{-1}$)×365 (subunits μm^{-1}).
Filaments lengths were measured for each processive construct to quantify processivity. The fraction of filaments bound to Fhod as a function of filament length was plotted and fit as an exponential decay in KaleidaGraph. The reciprocal of the fit was used to determine the characteristic run length. Off rates were calculated by the following equation: Off rate, k_{off} (s^{-1}) = elongation rate (subunits s^{-1}) / [characteristic run length, λ (μm)×365 (subunits μm^{-1})].

Chapter Three: Results

3.1 Fhod isoforms and mutants accelerate actin activity

To test the overall potency of each construct in the presence of actin we performed pyrene-labeled actin polymerization assays. All the tested constructs increased actin assembly compared to actin alone (Figure 3.1). The three isoforms differed in their ability to assemble actin, with Fhod-B showing the greatest activity (Figure 3.1A). The Fhod-A tail truncations all showed increased activity compared to Fhod-A and the activity of the Fhod-A tail truncation constructs gradually increased as the number of residues truncated increased (Figure 3.1B).

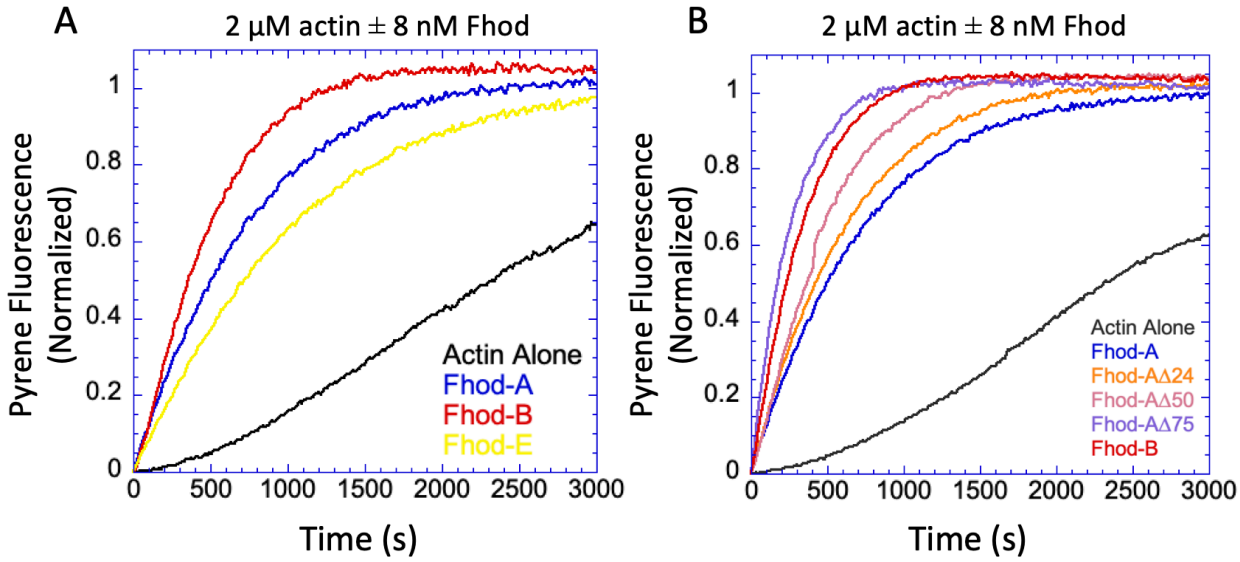

Figure 3.1: Fhod isoforms and Fhod-A tail truncation constructs accelerate actin assembly. *A-B,* assembly of 2 µM (10% pyrene-labeled) actin with 8 nM of indicated Fhod constructs.

We quantified the polymerization rate at $t_{1/2}$, relative to actin alone. Fhod-A and Fhod-E showed rates of 2.30 and 1.84 a.u. s^{-1}, respectively. The polymerization at $t_{1/2}$ was increased for Fhod-B compared to both Fhod-A and Fhod-E with a rate of 6.59 a.u. s^{-1} (Table 3.1, p. 20). The rate of polymerization at $t_{1/2}$ was calculated for each of the mutants and are displayed in Table 3.1 (p. 20).

3.2 Fhod isoforms differ in their contribution to actin elongation

Actin elongation was measured in the presence of preformed filaments (seeds) and profilin to determine the effect of Fhod-B on actin elongation rate (Figure 3.2A). The relative elongation rates were quantified for varying Fhod-B concentrations. Fhod-B showed an increase in elongation rate compared to actin alone. We fit the data with a binding equation and the affinity of Fhod-B for the barbed-ends was determined to be 4.6 nM. For comparison, the previously published effect of Fhod-A on actin elongation is included (Figure 3.2B; Patel et al., 2018). Fhod-A does not increase the elongation rate relative to actin alone in seeded elongation assays. Although it does appear to slow the elongation rate, we attribute this to artifacts from the fluorescence due to excessive actin bundling in the presence of higher Fhod-A concentrations.

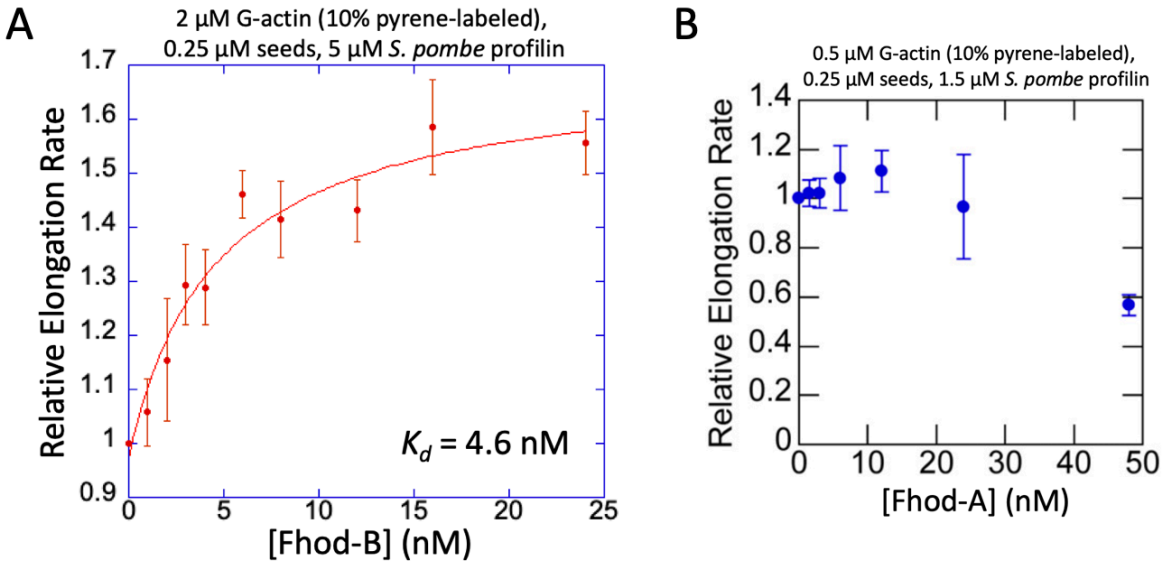

Figure 3.2: Fhod-B accelerates barbed-end elongation. *A,* quantification of elongation rates from four independent actin elongation experiments performed from preformed seeds in the presence of Fhod-B. Final conditions were 2 μM G-actin (10% pyrene-labeled), 0.25 μM F-actin seeds (~0.4 nM barbed-ends), 5 μM *S. pombe* profilin, and 1-24 nM Fhod-B. The data are the mean ± standard deviation from four independent experiments. The Fhod-B K_d value was determined from the binding equation to be 4.6 nM. *B*, quantification of elongation rates from three independent actin elongation experiments performed from preformed seeds in the presence of Fhod-A. Final conditions were 0.5 μM G-actin (10% pyrene-labeled), 0.25 μM F-actin seeds (~0.4 nM barbed-ends), and 1.5-48 nM Fhod-A. *Note:* Figure 3.2B is reprinted from (Patel et al., 2018).

TIRF microscopy was utilized to visualize individual growing actin filaments in the presence of different Fhod constructs. We measured filament elongation rates in the presence of 1 μM Mg^{2+}-G-actin (20% Oregon green-labeled). To identify elongating filaments bound to Fhod, we exploited the preferential binding of Chic to non-labeled actin. Only bright filaments are observed in the absence of Fhod and in the presence of either Fhod-A or Fhod-E. In contrast, in the presence of Fhod-B two populations of filaments are observed. One population consists of bright, short filaments and the other population consists of dim, long filaments (Figure 3.3A). Some of the dim filaments have bright ends which indicates Fhod-B dissociating from the growing filament. Although bundling was not quantified, it should be noted that bundles were only observed in the presence of Fhod-A at the concentrations measured (Figure 3.3A).

The length of individual filaments was measured over time to determine differences in elongation rates. Actin in the absence of Fhod assembled at a rate of 5.5 ± 1.0 subunits s^{-1}. Actin in the presence of either Fhod-A or Fhod-E resulted in elongation rates of 7.4 ± 0.9 and 5.3 ± 2.0 subunits s^{-1}, respectively (Figure 3.3B, 3.3C, and 3.3E). The bright filaments in the field of view when in the presence of Fhod-B also resulted in elongation rates comparable to actin alone. However, the dim filament population resulted in an accelerated elongation rate of 17.0 ± 2.4 subunits s^{-1} (Figure 3.3D), 3-fold faster compared to actin alone. A summary of these data is available in Table 3.1 (p. 20).

There was no statistical significance in elongation rate between actin alone, Fhod-A, Fhod-E, and the bright filament population observed in the presence of Fhod-B (Figure 3.5A and 3.5B). However, the difference in actin elongation rate of the dim filament population in the presence of Fhod-B was significant when compared to actin alone, Fhod-A, and Fhod-E (Figure 3.5B).

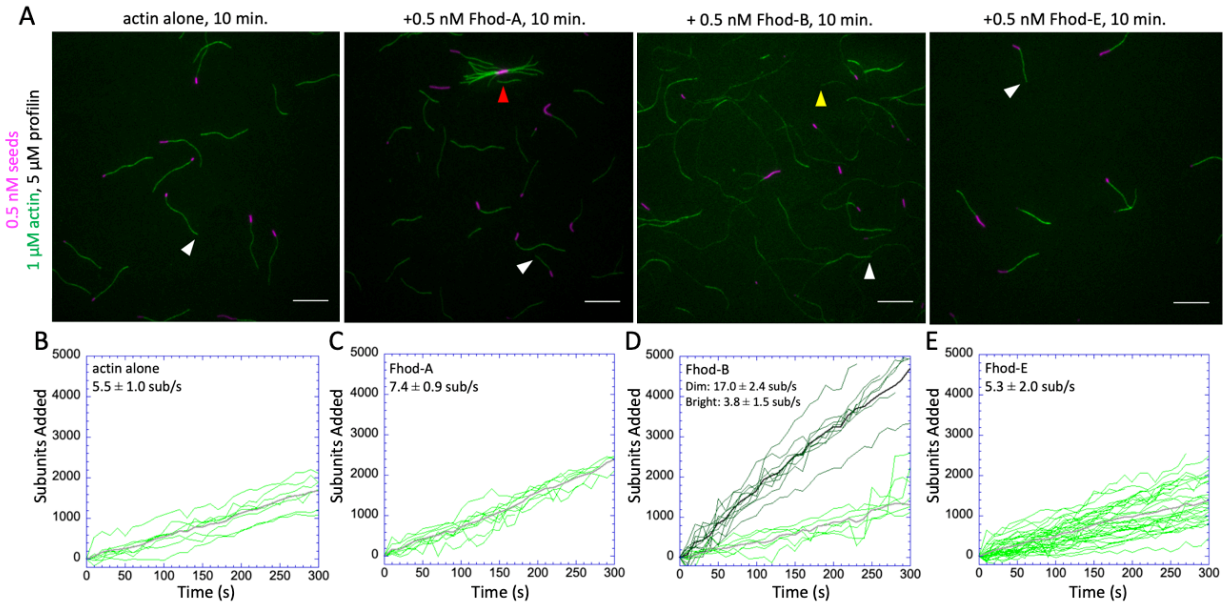

Figure 3.3: Tail regions influence filament elongation rate. *A,* direct observation of barbed-end elongation by TIRF microscopy with 0.5 nM seeds (1% biotinylated, labeled with Alexa Fluor 647-phalloidin; fuchsia), 1 µM G-actin (20% Oregon green-labeled; green), 5 µM Chic, ± 0.5 nM indicated Fhod construct. White arrows denote the barbed-ends of bright, slow-growing filaments (no Fhod bound). Yellow arrows denote the barbed-ends of dim, fast-growing filaments (Fhod bound). Red arrow denotes actin bundle. Images shown were taken 10 min after the start of polymerization. *Scale bars,* 10 µm. *B-E,* quantification of elongation from *A*. Bright green traces denote bright, slow-growing filaments (no Fhod bound). Dark green traces denote dim, fast-growing filaments (Fhod bound). Thick light and dark grey traces denote mean of the bright and dim growing populations, respectively. Elongation rates are the mean ± standard deviation from ≥ 2 flow chambers for each condition (n = 16, actin alone; n = 9, Fhod-A; n = 10 [dim] and n = 6 [bright], Fhod-B; n = 27, Fhod-E).

3.3 Fhod-A tail truncations accelerate actin elongation

To determine how the Fhod tail contributes to the differences observed between the splice isoforms' processivity we directly observed barbed-end elongation of the truncation constructs in the presence of 1 µM Mg^{2+}-G-actin (20% Oregon green-labeled) via TIRF microscopy. All the Fhod-A tail truncations showed both bright and dim filament populations (Figure 3.4A). Single filament measurements were taken over time. Similar to Fhod-B, actin in the presence of the truncated Fhod-A mutants resulted in two populations of elongation rates. The bright filaments elongated at rates comparable to actin alone, whereas the dim filaments

elongated ~3-fold faster than actin alone (Figure 3.4B-D). Specifically, actin in the presence of either Fhod-AΔ24, Fhod-AΔ50, or Fhod-AΔ75 elongated at rates of 13.3 ± 2.3, 14.7 ± 2.4, and 14.1 ± 2.8 subunits s^{-1}, respectively (Figure 3.4B-D). Interestingly, these rates are indistinguishable from those with Fhod-B.

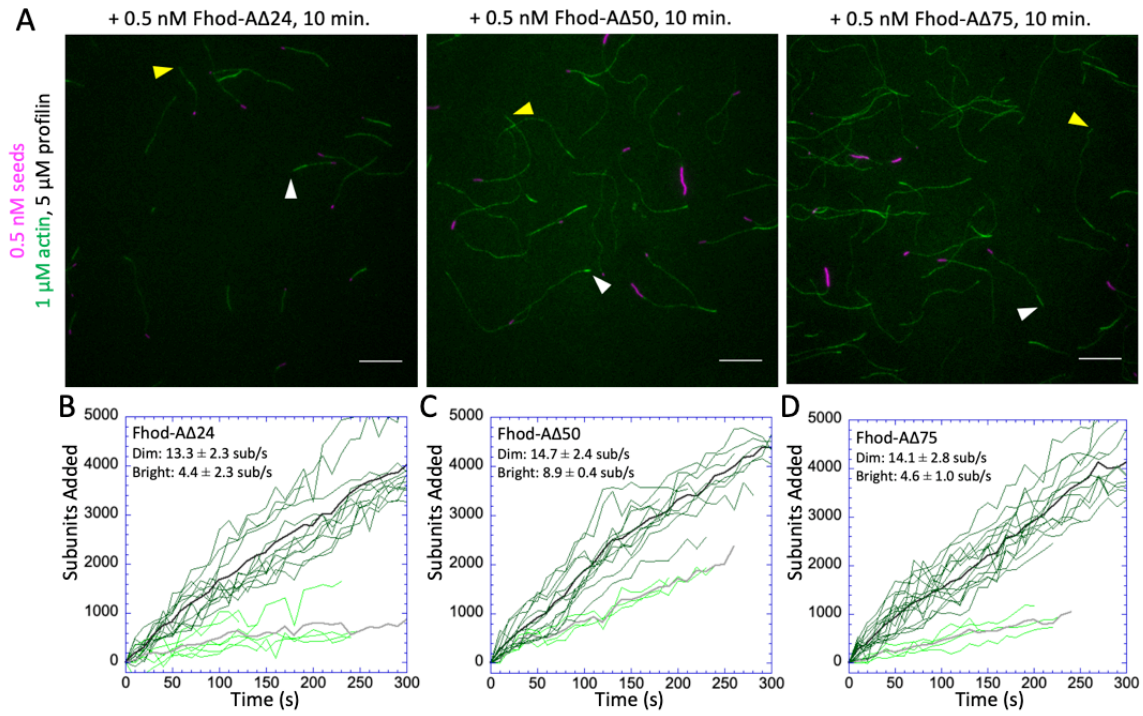

Figure 3.4: Fhod-A C-terminally truncated constructs accelerate actin elongation rate. *A,* direct observation of barbed-end elongation by TIRF microscopy with 0.5 nM seeds (1% biotinylated, labeled with Alexa Fluor 647-phalloidin; fuchsia), 1 µM G-actin (20% Oregon green-labeled; green), 5 µM Chic, ± 0.5 nM indicated Fhod construct. White arrows denote the barbed-ends of bright, slow-growing filaments (no Fhod bound). Yellow arrows denote the barbed-ends of dim, fast-growing filaments (Fhod bound). Images were taken 10 min after the start of polymerization. *Scale bars,* 10 µm. *B-D,* quantification of elongation from *A*. Bright green traces denote bright, slow-growing filaments (no Fhod bound). Dark green traces denote dim, fast-growing filaments (Fhod bound). Thick light and dark grey traces denote mean of the bright and dim growing populations, respectfully. Elongation rates are the mean ± standard deviation from ≥ 2 flow chambers for each condition (n = 12 [dim] and n = 6 [bright], Fhod-AΔ24; n = 12 [dim] and n = 3 [bright], Fhod-AΔ50; n = 16 [dim] and n = 4 [bright], Fhod-AΔ75).

Statistical analysis reveals that the elongation rates of dim, fast-growing filaments and bright, slow-growing filaments were significantly different for each of the Fhod-A tail truncations. There was no statistical difference found between actin alone and the bright, slow-

growing filaments found in the presence of these constructs (Figure 3.5A). A significant difference in elongation rate was determined between the actin alone and the dim, fast-growing filaments observed in the presence of the Fhod-A tail truncations (Figure 3.5B). The difference in elongation rates between the Fhod-A tail truncations showed no significance. Though some minor differences were determined between Fhod-B and some of the Fhod-A tail truncations, there was no gradual trend correlating with the gradual truncation of the Fhod-A tail (Figure 3.5B).

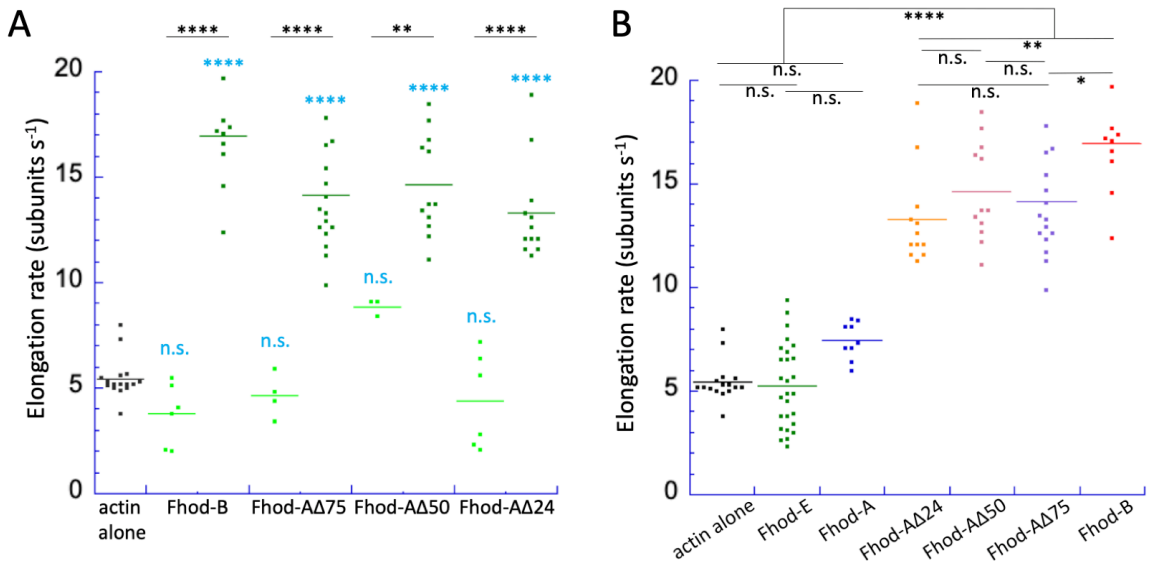

Figure 3.5: Differences in elongation rate. *A,* quantification of elongation rates for constructs found to have two populations of elongation rates. Bright filament populations are shown in bright green and dim filament populations are shown in dark green. Statistical analysis results compared to actin alone are shown in light blue. *B,* quantification of elongation rates for Fhod isoforms and C-terminal truncated Fhod-A mutants. Dim filament population elongation rates were used for constructs that had two elongation rate populations. *Data for this figure was taken from Figure 3.3 and Figure 3.4.* The *p* values were calculated using the one-way ANOVA with post-hoc Tukey Honestly Significant Difference Test. ****$p < 10^{-4}$, **$p < 10^{-2}$, *$p < 0.05$.

3.4 Fhod-B and Fhod-A tail truncation mutants are processive

To better understand how the tail domain influences the association of Fhod to the barbed-end of growing filaments we used TIRF microscopy to quantify differences in

processivity. Fhod-bound filament lengths were measured for Fhod-B and Fhod-A tail truncations to determine characteristic run lengths. Dim filaments were measured and dissociation was determined by the observation of a dim, fast-growing filament switching to a bright, slow-growing filament. The fraction of filaments bound to Fhod was determined as a function of filament length and the data were fit to an exponential decay to obtain the characteristic run lengths for each construct (Figure 3.6A). The characteristic run length is defined as the elongation rate/k_{off} and is a measure of how long a formin remains associated with a growing filament. A faster decay was observed for the Fhod-A tail truncations than Fhod-B. The fit resulted in a characteristic run length of 94 ± 6 μm for Fhod-B, whereas the Fhod-A tail truncations ranged from 37-45 μm.

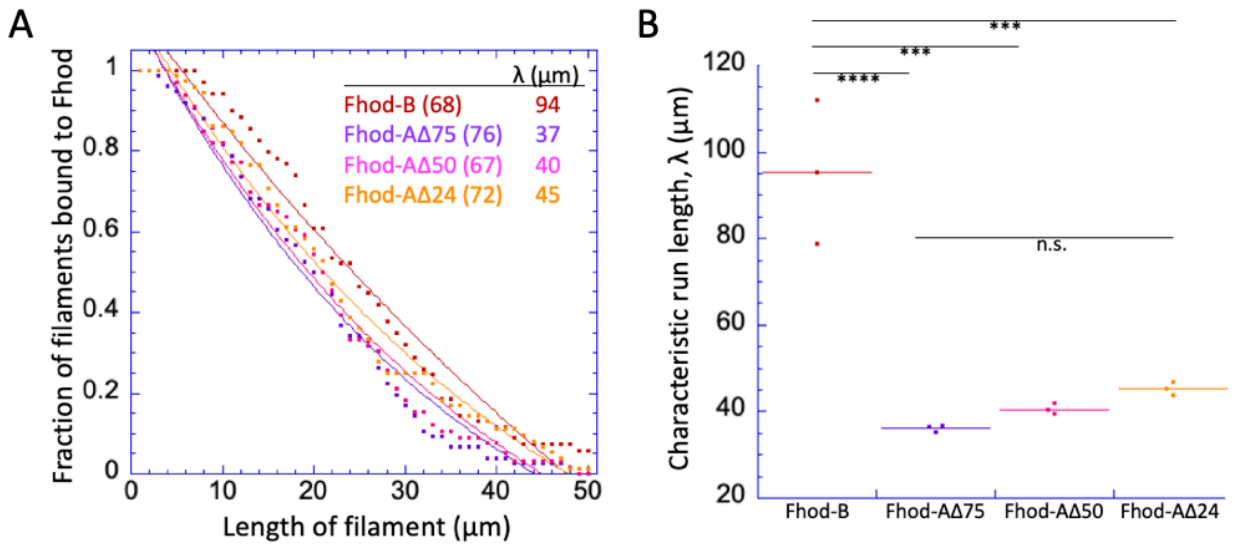

Figure 3.6: Determination of characteristic run length, λ, for Fhod-B and Fhod-A tail truncations. *A,* quantification of processivity shown as a decay plot. Data points represent the averages from three data replicates taken from separate experiments. The total number of filaments analyzed for each construct is shown in parentheses. The solid lines represent the exponential curve fits of the data used to determine the characteristic run length. *B,* the characteristic run length for each data collection. Averages for each construct are represented by a line. The *p* values were calculated using the one-way ANOVA with post-hoc Tukey Honestly Significant Difference Test. ****$p < 10^{-4}$, ***$p < 10^{-3}$.

Analysis was performed on the characteristic run lengths to determine statistical differences between constructs (Figure 3.6B). There was no significant difference in characteristic run length found between the Fhod-A tail truncations. Though there was a significant difference between Fhod-B and the Fhod-A tail truncations, there was no trend of increased processivity as the tail was gradually truncated.

3.5 Summary of the results

A comparison of the parameters tested in this study is presented in Table 3.1. The off rates (k_{off}) for the processive constructs were calculated from the measured elongation rate and characteristic run length for each construct.

	Polymerization rate[a] at $t_{1/2}$ (a.u. s^{-1})	**Elongation rate (subunits s^{-1})**	**k_{off} x 10^{-5} (s^{-1}) [b]**	**Characteristic run length (μm)**
Fhod-A	2.30	7.4 ± 0.9	n.d.	2[c]
Fhod-AΔ24	2.33	13.3 ± 2.3	81.0 ± 15.2	45 ± 3
Fhod-AΔ50	3.31	14.6 ± 2.4	100.0 ± 17.0	40 ± 2
Fhod-AΔ75	6.85	14.1 ± 2.8	104.4 ± 21.4	37 ± 2
Fhod-B	6.59	17.0 ± 2.4	49.5 ± 7.7	94 ± 6
Fhod-E	1.84	5.3 ± 2.0	n.d.	n.d.
actin alone	1.00	5.5 ± 1.0	n.a.	n.a.

Table 3.1: Summary table
[a] Relative to actin alone
[b] k_{off} = elongation rate (subunits s^{-1}) / [characteristic run length, λ (μm)×365 (subunits μm^{-1})]
[c] Data from (Patel et al., 2018)
n.d. = not done
n.a. = not applicable

Chapter Four: Discussion

4.1 The role of the formin tail

Previously, we found that Fhod isoform A (Fhod-A) exhibits classic formin activities such as potent nucleation and the capacity to bundle filaments. However, it is only weakly processive and does not enhance the elongation rate (Patel et al., 2018). *Drosophila* Fhod is alternatively spliced into eight isoforms, four that differ only in the region C-terminal to the FH2 domain, which has been loosely defined as the tail. Our lab has extensively characterized another formin, Cappuccino (Capu), and found that the tail region influences nucleation and processivity via direct interaction with growing actin filaments (Vizcarra et al., 2014). This work showed that gradual truncation of the Capu tail resulted in a corresponding decrease in nucleation and processivity. However, the tail did not influence elongation rate. A model for the interaction between the Capu tail and growing filaments was developed. In this model, it was posited that the FH2 domain's association with the barbed-ends of filaments is enhanced by a weak interaction between the Capu tail and the sides of filaments. Essentially, during dissociation of the FH2 domain, the weak electrostatic interaction of the tail and filament created a tether, re-stabilizing the interaction with the FH2 domain and the barbed-end. Other formin tails have been implicated in nucleation and processivity (Gould et al., 2011; Vizcarra et al. 2014). We hypothesized that the Fhod tail makes important contributions to processivity and nucleation, based on the number of splice isoforms that differ only in their tail domains.

Processivity is the time a formin remains associated with a growing filament. The elongation rate and processivity determine the average length of filaments built by formins. We were initially surprised to find that Fhod-A is very weakly processive, with a characteristic run

length of 2 μm (Patel et al., 2014). In contrast, Capu has a characteristic run length of 300 μm (Yoo et al., 2015). The length of the tail domains of Fhod-A and Capu greatly differ at 129 and 30 residues, respectively. Due to the differences in elongation between Capu and Fhod-A, we hypothesized that the long tail of Fhod-A interferes with Fhod's ability to remain processively associated with growing filaments. In this work, we compare Fhod-A-mediated actin assembly with two additional Fhod isoforms, B and E (Fhod-B and Fhod-E). The Fhod-B tail length is only 30 residues, the same length as the Capu tail and 99-amino acids shorter than the Fhod-A tail. The Fhod-E tail is similar in length to the Fhod-A tail with 123 residues. The first 105 residues of the Fhod-A and Fhod-E tails are identical (Figure 1.4). Although both isoforms contain a considerable number of basic residues in the remaining tail, there is a lot of variation in sequence between the two. While the C-terminal tails of Fhod-A, -B, and –E vary, their FH1 and FH2 domains are identical, making this an ideal system in which to study the role of the formin tail.

To test the effect of the Fhod tail we also produced Fhod-A tail truncation constructs that were intermediate in length between Fhod-A and Fhod-B (Figure 1.4). We reasoned that if the length of the tail was interfering with growing filaments and this was the dominant contribution to processivity, we would see a gradual change in processivity that corresponded to the number of residues truncated.

4.2 Fhod tails contribute to difference in actin activity

We found that Fhod-A, -B, and -E have measurably different effects on overall actin assembly in bulk assays (Figure 3.1A). Fhod-B was the most potent of the three isoforms, suggesting that the longer tails somehow decrease actin assembly. Additionally, Fhod-B was observed to accelerate elongation rate compared to actin alone in bulk assays (Figure 3.2A),

demonstrating that the Fhod-FH1FH2 region is capable of accelerating elongation and further suggesting that the longer tails are decreasing actin assembly activities.

Differences in overall activity between the isoforms may be indicative of altered nucleation in addition to elongation. The effect of these isoforms on nucleation remains to be tested. The difference in activity, observed in the pyrene assay (Figure 3.1A), between Fhod-A and Fhod-E is likely to be in their ability to nucleate actin, based on the fact that neither accelerated elongation. The tails of Capu and mDia1 both contribute to nucleation by a poorly understood mechanism (Gould et al. 2011; Vizcarra et al., 2014). It is possible the tail domain is involved in assisting the FH2 domain in the stabilization of the rapidly dissociating actin dimers and trimers.

In bulk assays, the Fhod-A tail truncations display a correlation between increased actin activity and a shorter tail (Figure 3.1B). However, single filament assays using TIRF microscopy did not reveal a gradual difference in acceleration of elongation or degree of processivity. Instead there was a marked change when the last 24 residues were removed from Fhod-A (Figures 3.5B and 3.6B). Then there was little change until the tail was reduced to that of Fhod-B. Thus, some of the differences observed in the pyrene assay is likely to be due to differences in nucleation strength. We conclude that Fhod tails tune nucleation and processivity as has been determined for other formins.

4.3 Potential mechanisms of Fhod tail in altering processivity

We have considered several possible mechanisms of how the longer Fhod tails diminish processivity. First, we have considered possible interactions between the longer tails and the sides of filament. The interaction of the tail with the sides of filaments may either be too weak or too strong to allow for sustained barbed-end association. If the interaction between the tail and

the filament side is too weak, a nonspecific electrostatic tether to the filament may not exist. Thus, Fhod isoforms with longer tails may quickly diffuse away from the filament after barbed-end dissociation events, hindering FH2 and barbed-end re-association. Alternatively, if the interaction between the tail and the sides of filaments is too strong, filament side binding may outcompete barbed-end binding, leading to barbed-end dissociation. We have also considered that the longer Fhod tails are sterically clashing with the filament and contributing to an increase in barbed-end dissociation events. Yet another possibility is that the Fhod tail may be interacting with the FH2 domain, interfering with barbed-end binding. We initially asked if the longer Fhod tails adopt secondary structure facilitating these possible interactions, but have since ruled this out based on circular dichroism experiments (data not shown).

Previously, our lab found that chimeras using the Capu FH1-FH2 and the tails of other formin alter processivity (Vizcarra et al., 2014). Chimeras with the Capu FH1-FH2 domain and mDia1 or mDia2 domain increase processivity slightly compared to Capu wild-type. In contrast, chimeras with the Capu FH1-FH2 domain and the FMNL1 tail substantially decrease processivity. The mDia1, mDia2, and FMNL1 tails all extend beyond the Capu tail with lengths of 106, 162, and 57 residues, respectively. However, the extent to which these chimeras alter processivity does not favor a model in which steric hindrance due to tail lengths contributes to the loss of processivity. The Capu-FMNL1 chimera decreases processivity and contains the shortest tail length of these chimeras. This along with our work probing differences in processivity through gradually truncating the Fhod tail (Figure 3.6) favors a model in which the tail is directly interacting with the filament side. We reasoned that the longer Fhod-A and Fhod-E tails interact strongly with the sides of filaments. The longer Fhod-A and Fhod-E tails contain many basic residues. These residues may increase the interaction between the tail and the sides

of filaments. If the affinity for side binding was substantially increased compared to the affinity to the barbed-end, the tail would bind strongly to the sides of filaments leading to dissociation at the barbed-end. This differs from the model proposed for Capu by which the tail's interaction stabilizes the FH2 domain's association with the growing filament (Vizcarra et al., 2014).

Interestingly, Fhod-A was the only construct to show bundling in the TIRF microscopy experiments at the concentrations tested. It is possible Fhod-A is binding the sides of filaments to facilitate bundling which may have physiological significance *in vivo*. In contrast, bundling is not observed in the presence of Fhod-E at the same concentrations. This suggests that the mechanism by which the Fhod-A and Fhod-E tail contribute to the loss of processivity may differ. However, it is also possible that the Fhod-E tail does strongly bind the sides of filaments but does not strongly bundle filaments.

We recently identified a conserved sequence between Fhod-A and human homologs, Fhod1 and Fhod3, extending 9 residues beyond our Fhod-AΔ24 construct. Our preliminary work suggests that neither Fhod1 nor Fhod3 is highly processive. This finding provides potential insight into why the Fhod-AΔ24 construct behaves so differently from the full length Fhod-A tail construct. This conserved region is highly phosphorylated in mammals (Takeya et al., 2008). It is intriguing to think that phosphorylation alters processivity or filament side binding and bundling activity.

4.4 Physiological relevance

Fhod has been implicated in many different cellular processes in *Drosophila* such as wing and tracheal development, macrophage motility, sarcomere organization, and cardiac contractility (Wooten et al., 2013; Lammel et al., 2014; Shwartz et al., 2016; Bechtold et al., 2014). The differences in activity levels conferred by the C-terminal tail of Fhod splice variants

may contribute to Fhod's ability to build diverse actin structures in these varied tissue types. It has been determined that Capu is essential for establishing polarity during oocyte development in *Drosophila* and that loss of Capu results in sterile females (Emmons et al., 1995; Manseau & Schüpbach, 1989). As such, it was suggested that the high processivity of Capu may be important to facilitate building an actin meshwork that spans the large *Drosophila* oocyte (Vizcarra et al., 2014). It is therefore reasonable to speculate, based on our findings, that Fhod-B is expressed for the assembly of longer actin filaments, whereas Fhod-A and -E may be expressed for the assembly of shorter filaments.

In general, FHOD family proteins localize to relatively short actin filaments, such as in stress fibers and sarcomeres. Fhod-A may also be important to produce actin bundles as it appears to be a much stronger bundler than the other isoforms. We previously found Fhod-A to have an affinity of 0.18 μM for the sides of actin filaments (Patel et al., 2018). Consistent with the possibility that strong bundling by Fhod-A is mediated by the tail region unique to Fhod-A, the last 24 residues, none of the Fhod-A tail truncation constructs produce visible actin bundles (Figure 3.4A).

4.5 Future Directions

In addition to continued biochemical characterization of the Fhod tails, in the future we hope to further explore the differences in Fhod isoform expression by RT-PCR and *in vivo* genetic analysis. We will look at specific tissue types such as muscle, ovaries, brain, and hemolymph to determine differences in isoform expression. It was previously determined that flies expressing only Fhod isoform A are viable (Lammel, et al., 2014). This indicates that though the other isoforms may be important for building specific actin structures, they are not necessary for viability. For example, either isoform H or I is necessary for proper muscle

development (Shwartz et al., 2016). Isoforms H and I differ in their N-termini and are otherwise identical to Fhod-A, including sharing the same tail. Fhod-A was found to localize to the sarcomere M-lines, whereas isoform H was found to localize exclusively to Z-discs (Shwartz et al. 2016). The weak processivity shared by the Fhod-A and -E tails may be relevant for building short actin filaments in the sarcomere of muscle tissues. In contrast, Fhod-B may have similar localization to Capu and be relevant for building large meshworks that span large cells. Additionally, Fhod-B does not contain the DAD domain which functions in auto-inhibition. Thus, the mechanism of regulation between the isoforms may differ *in vivo.* The function of Fhod-B may be regulated by expression and degradation and it may serve a more transient purpose than the other isoforms such as in macrophage migration.

Ultimately we aim to link differences in the tail to their contributions to different actin structures. We will determine how the tail interacts with growing filaments to attenuate actin polymerization *in vivo.* This work will further our understanding of Fhod- and formin-mediated actin structures.

References

Al Haj, A., Mazur, A.J., Radaszkiewicz, K., Radaszkiewicz, T., Makowiecka, A., Stopschinski, B.E., Schönichen, A., Geyer, M., and Mannherz, H.G. (2015). Distribution of formins in cardiac muscle: FHOD1 is a component of intercalated discs and costameres. *Eur J Cell Biol* **94**, 101-113.

Arimura, T., Takeya, R., Ishikawa, T., Yamano, T., Matsuo, A., Tatsumi T., Nomura, T., Sumimoto, H., and Kimura, A. (2013). Dilated cardiomyopathy-associated FHOD3 variant impairs the ability to induce activation of transcription factor serum response factor. *Circ J* **77**, 2990-2996.

Bechtold, M., Schultz, J., and Bogdan, S. (2014). FHOD proteins in actin dynamics- a formin' class of its own. *Small GTPases* **5**, 651-656.

Bor, B., Vizcarra, C.L., Phillips, M.L., and Quinlan, M.E. (2012). Autoinhibition of the formin Cappuccino in the absence of canonical autoinhibitiory domains. *Mol Biol Cell* **23**, 3801-3813.

Chang, F., Drubin, D., and Nurse, P. (1997). cdc12p, a protein required for cytokinesis in fission yeast, is a component of the cell division ring and interacts with profilin. *J Biol Chem* **137**, 169-182.

Chhabra, E.S. and Higgs, H.N. (2007). The many faces of actin: matching assembly factors with cellular structures. *Nat Cell Bio* **9**, 1110-1121.

Courtemanche, N. and Pollard, T.D. (2012). Determinants of Formin Homology 1 (FH1) domain function in actin filament elongation by formins. *J Biol Chem* **287**, 7812-7820.

Doolittle, L.K., Rosen, M.K., and Padrick, S.B. (2013) Measurement and analysis of *in vitro* actin polymerization. *Methods Mol Biol* **1046**, 273-293.

Dwyer, J., Pluess, M., Iskratsch, T., dos Remedios, C.G., and Ehler, E. (2014). The formin FHOD1 in cardiomyocytes. *Anat Rec (Hoboken)* **297**, 1560-1570.

Emmons, S., Phan, H., Calley, J., Chen, W., James, B., and Manseau, L. (1995). Cappuccino, a *Drosophila* maternal effect gene required for polarity of the egg and embryo, is related to the vertebrate *limb deformity* locus. *Genes Dev* **9**, 2482-2494.

Goode, B.L. and Eck, M.J. (2007). Mechanism and function on formins in the control of actin assembly. *Annu Rev Biochem* **76**, 593-627.

Gould, C.J., Maiti S., Michelot, A., Graziano, B.R., Blanchoin, L., and Goode, B.L. (2011) The formin DAD domain plays dual roles in autoinhibition and actin nucleation. *Curr Biol* **21**, 384-390.

Higgs, H.N. (2005). Formin proteins: a domain-based approach. *Trends in Biochem Sci* **30**, 342-353.

Holmes, K.C., Popp, D., Gebhard, W., and Kabsch, W. (1990). Atomic model of the actin filament. *Nature* **347**, 44-49.

Iskratsch, T., Lange, S., Dwyer, J., Kho, A.L., dos Remedious, C., and Ehler, E. (2010). Formin follows function: a muscle-specific isoform of FHOD3 is regulated by CK2 phosphorylation and promotes myofibril maintenance. *J Cell Biol* **191**, 1159-1172.

Jurmeister, S., Baumann, M., Balwierz, A., Keklikoglou, I., Ward, A., Uhlmann, S., Zhang, J.D., Wiemann, S., and Sahin, Ö. (2012). MicroRNA-200c represses migration and invasion of breast cancer cells by targeting actin-regulatory proetins FHOD1 and PPM1F. *Mol Cell Bio* **32***,* 633-651.

Kovar, D.R., Harris, E.S., Mahaffy, R., Higgs, H.N., and Pollard, T.D. (2006). Control of the assembly of ATP- and ADP-actin by formins and profilin. *Cell* **124**, 423-435.

Krainer, E.C., Ouderkirk, J.L., Miller, E.W., Miller, M.R., Mersich, A.T., and Blystone, S.D. (2013). The multiplicity of human formins: Expression patterns in cells and tissues. *Cytoskeleton (Hoboken)* **70**, 424-438.

Lammel, U., Bechtold, M., Risse B., Berh, D., Fleige, A., Bunse, I., Jiang, X., Klämbt, C., and Bogdan, S. (2014). The Drosophila FHOD1-like formin Knittrig acts through Rok to promote stress fiber formation and directed macrophage migration during the cellular immune response. *Development* **141**, 1366-1380.

Li, C., Wen, A., Shen, B., Lu, J., Huang, Y., and Chang, Y. (2011). FastCloning: a highly simplified, purification-free, sequence- and ligation-independent PCR cloning method. *BMC Biotechnol* **11**, 1-10.

Li, F. and Higgs, H.N. (2005). Dissecting requirements for auto-inhibition of actin nucleation by the formin, mDia1. *J Biol Chem* **280**, 6986-6992.

Manseau, L.J. and Schüpback, T. (1989). Cappuccino and spire: two unique maternal-effect loci required for both the anteroposterior and dorsoventral patterns of the *Drosophila* embryo. *Genes Dev* **3**, 1437-1452.

Monzo, P., Chong, Y.K., Guetta-Terrier, C., Krishnasamy, A., Sathe, S.R., Yim, E.K.F., Ng, W.H., Ang, B.T., Tang, C., Ladoux, B., Gauthier, N.C., and Sheetzm M.P. (2016). Mechanical confinement triggers glioma linear migration dependent on formin FHOD3. *Mol Biol Cell* **27**, 1246-1261.

Oda, T., Iwasa, M., Aihara, T., Maéda, Y., and Narita, A. (2009). The nature of the globular- to fibrous-actin transition. *Nature* **457**, 441-445.

Patel, A.A., Oztug Durer, Z.A., van Loon, A.P., Bremer, K.V., and Quinlan, M.E. (2018). *Drosophila* and human FHOD family formins nucleate actin filaments. *J Biol Chem* **293**, 532-540.

Paul, A. and Pollard, T. (2008). The role of the FH1 domain and profilin in formin-mediated actin- filament elongation and nucleation. *Curr Biol* **18**, 9-19.

Paul, N.R., Allen J.L., Chapman, A., Morlan-Mairal, M., Zindy, E., Jacquemet, G., Fernandex del Ama, L., Ferizovic, N., Green, D.M., Howe, J.D., Ehler, E., Hurlstone, A., and Caswell, P.T. (2015). α5β1 integrin recycling promotes Arp2/3-independent cancer cell invasion via the formin FHOD3. *J Cell Biol* **210**, 1013-1031.

Pollard, T.D. and Cooper, J.A. (2009). Actin, a Central Player in Cell Shape and Movement. *Science* **326**, 1208-1212.

Randall, T.S. and Ehler, E. (2014). A formin-g role during development and disease. *Eur J Cell Biol* **93**, 205-211.

Schönichen, A. and Geyer, M. (2010). Fiften formins for an actin filament: a molecular view on the regulation of human formins. *Biochim Biophys Acta* **2**, 152-163.

Schönichen, A., Mannherz, H.G., Behrmann, E., Mazur, A.J., Kühn, S., Silván, U., Schoenenberger, C.-A., Frackler, O.T., Raunser, S., Dehmelt, L., and Geyer, M. (2013). FHOD1 is a combined actin filament capping and bundling factor that selectively associates with actin arcs and stress fibers. *J Cell Sci* **126**, 1891-1901.

Severson, A.F., Baillie, D.L., and Bowerman, B. (2002). A Formin Homology protein and a profilin are required for cytokinesis and Arp2/3-independent assembly of cortical microfilaments in *C. elegans*. *Curr Biol* **12**, 2066-2075.

Shwartz, A., Dhanyasi, N., Schejter, E., and Shilo, B.-Z. (2016). The *Drosophila* formin Fhos is a primary mediator of sarcomeric thin-filament array assembly. *eLife* **5**, 1-24.

Silkworth, W.T., Kunes, K.L., Nickel, G.C., Phillips, M.L., Quinlan, M.E., and Vizcarra, C.L. (2018). The neuron-specific formin Delphilin nucleates nonmuscle actin but does not enhance elongation. *Mol Biol Cell* **29**, 610-621.

Smith, M.B., Li, H., Shen, T., Huang X., Yusuf, E., and Vavylonis, D. (2010). Segmentation and tracking of cytoskeletal filaments using open active contours. *Cytoskeleton* **67**, 693-705.

Takeya, R., Taniguchi, K., Narumiya, S., and Sumimoto, H. (2008). The mammalian formin FHOD1 is activated through phosphorylation by ROCK and mediates thrombin-induced stress fibre formation in endothelial cells. *EMBO J* **27**, 618-628.

Vizcarra, C.L., Bor, B., and Quinlan, M.E. (2014). The role of formin tails in actin nucleation, processive elongation, and filament bundling. *J Biol Chem* **289**, 30602-30613.

Wooten E.C., Hebl, V.B., Wolf, M.J., Greytak, S.R., Orr, N.M., Draper, I., Calvino, J.E., Kapur, N.K., Maron, M.S., Kullo, I.J., Ommen S.R., Bos, J.M., Ackerman, M.J., and Huggins, G.S. (2013) Formin Homology 2 domain containing 3 variants associated with hypertrophic cardiomyopathy. *Circ Cardiovasc Genet* **6**, 10-18.

Yoo, H., Roth-Johnson, E.A., Bor, B., and Quinlan, M.E. (2015). *Drosophila* Cappuccino alleles provide insight into formin mechanism and role in oogenesis. *Mol Biol Cell* **26**, 1875-1886.